Student-Faculty Collaborative Research

8-29-2008

Time-averaged electronic speckle pattern interferometry in the presence of ambient motion. Part I: Theory and experiments

Thomas R. Moore
Department of Physics, Rollins College, TMOORE@rollins.edu

Jacob J. Skubal
Department of Physics, Rollins College

Follow this and additional works at: http://scholarship.rollins.edu/stud_fac

Part of the Physics Commons

Time-averaged electronic speckle pattern interferometry in the presence of ambient motion. Part I. Theory and experiments

Thomas R. Moore* and Jacob J. Skubal

Department of Physics, Rollins College, Winter Park, Florida 32789, USA

*Corresponding author: tmoore@rollins.edu

An electronic speckle pattern interferometer is introduced that can produce time-averaged interferograms of harmonically vibrating objects in instances where it is impractical to isolate the object from ambient vibrations. By subtracting two images of the oscillating object, rather than the more common technique of subtracting an image of the oscillating object from one of the static objects, interferograms are produced with excellent visibility even when the object is moving relative to the interferometer. This interferometer is analyzed theoretically and the theory is validated experimentally.   © 2008 Optical Society of America

OCIS codes: 120.6160, 120.7280, 330.4150.

1. Introduction

Electronic speckle pattern interferometry is a well-established technique and is commonly used to study the deflection of diffusely reflecting objects. These deflections may be due to static displacement, transient vibrations, or continuous harmonic motion [1,2]. This technique is often a desirable method of vibration analysis since it is sensitive to submicrometer motion, is both noncontact and nondestructive, and can be relatively inexpensive to implement.

Although high sensitivity is usually a desirable feature of interferometers, it is also problematic in speckle pattern interferometry, because increased sensitivity enhances the susceptibility to decorrelation of the interfering beams due to ambient vibrations. Low-frequency vibrations are notoriously difficult to suppress, and this problem is accentuated when studying large or weakly supported objects.

The problems associated with electronic speckle pattern interferometry in the presence of ambient vibrations have been the subject of discussion for some

time. However, the discussions usually center on methods to mitigate the effects of vibration either by isolation of the system or by limiting the sampling time of the detector [3]. While these methods are sometimes successful, implementation is usually costly and difficult, especially outside a laboratory environment.

Recently the problem of decorrelation of the two beams of an electronic speckle pattern interferometer due to low-frequency ambient vibrations was addressed within the context of studying the deflection shapes of a harmonically vibrating piano soundboard [4]. In these experiments the observation of fringe patterns corresponding to the deflection shapes of the harmonically vibrating object was complicated by ambient vibrations. These low-frequency vibrations resulted in the motion of the entire object despite semi-active vibration isolation of the support mechanisms. This motion was primarily due to the fact that the interferometer and object under study were mounted on separate supports, which was necessary due to the large size of the object. The resulting independent motion of the object and the interferometer caused the speckle pattern to change during the sampling time, resulting in the decorrelation of the

two speckle patterns, which must be subtracted to form the interferogram.

It was reported in [4] that the adverse effects attributable to the decorrelation of the object and reference beams could be overcome to some extent by modifying the image subtraction algorithm. In fact, the reported algorithm only produces interference fringes if a time-dependent phase shift exists between the two interfering beams. It was also suggested that for more stable objects, it may be advantageous to purposefully introduce such a phase shift. The authors also posited a theory explaining how this time-dependent phase shift of the beams could be advantageous but did not fully develop it. We do so here.

In what follows we discuss an electronic speckle pattern interferometer that images harmonically vibrating objects. After introducing the most simple version of the interferometer, we propose a design for an electronic speckle pattern interferometer that images harmonic vibrations in the presence of ambient motion. We derive a theory that describes the visibility of the interferograms produced by such an interferometer, followed by experimental evidence that the theory accurately predicts the output. Finally we discuss how this interferometer can be applied to objects undergoing harmonic motion both in the presence of and absence of ambient motion.

2. Theory

Electronic speckle pattern interferometers have been used for more than 35 years, and there are several different arrangements described in the literature. Here we concentrate only on the design useful for imaging harmonically vibrating objects and specifically on the most simple design. Those interested in the many imaginative and useful variations on this simple arrangement should consult [1,2] and the references therein.

A. Electronic Speckle Pattern Interferometer

The most simple arrangement of an electronic speckle pattern interferometer is shown schematically in Fig. 1 [5,6]. Two coherent beams are simultaneously imaged onto a detector: the object beam, which is derived from light reflected from a dif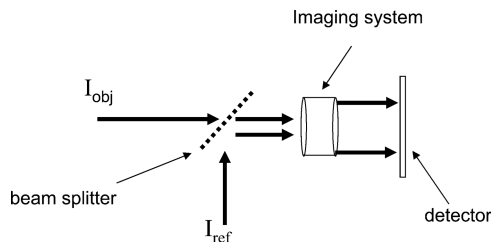fusely reflecting, harmonically vibrating object, and the reference beam, which is directly transmitted to the detector without being reflected from the object. Typically the detector is a charge-coupled device (CCD) array with an integration time that is much greater than the period of the harmonic motion of the object.

In the following analysis we consider the response of only an infinitesimal portion of the recording device, and therefore we can treat both the object and the reference beams as plane waves. Thus the intensity at a point on the detector may be described by the usual equation for two-beam interference, i.e.,

$$I = I_{obj} + I_{ref} + 2\sqrt{I_{obj}I_{ref}} \cos\phi, \qquad (1)$$

where I_{obj} and I_{ref} are the intensities of the object and reference beams, respectively, and ϕ is the phase difference between the two beams.

Speckle pattern interferometric studies of harmonically vibrating objects involve a time-varying phase difference between the object and the reference beams. We follow the usual method of analysis by assuming that the surface of the object illuminated by the object beam moves with simple harmonic motion at some angular frequency ω_0. The phase difference between the object and the reference beams during deformation of the surface of the object can then be expressed as

$$\phi = \phi_0 + \xi \sin\omega_0 t, \qquad (2)$$

where ϕ_0 is the initial phase difference between the two beams. Parameter ξ is the amplitude of the time-varying phase due to the motion of the object's surface given by

$$\xi = \frac{2\pi\Delta z}{\lambda}(\cos\theta_i + \cos\theta_r), \qquad (3)$$

where λ is the wavelength of the illuminating light, Δz is the amplitude of the object's surface displacement, and θ_i and θ_r are the incident and reflected angles of the object beam, respectively.

Substituting Eq. (2) into Eq. (1) yields an equation for the time-varying intensity of a point on the detector:

$$I_1 = I_{obj} + I_{ref} + 2\sqrt{I_{obj}I_{ref}} \cos[\phi_0 + \xi \sin\omega_0 t]. \qquad (4)$$

While Eq. (4) describes the instantaneous intensity at the detector, the interference pattern resulting from the coincidence of the object and the reference beams is normally recorded by a device that has an integration time that is long compared to the period of the motion of the object. Therefore, the recorded image represents a time average of the interference. Provided that the intensities of the two beams are time independent, the intensity recorded by the detector can be described as

Fig. 1. Simple schematic of an electronic speckle pattern interferometer. The object beam with intensity I_{obj} originates with light reflected from a harmonically vibrating object. The reference beam with intensity I_{ref} is coherent with the object beam but has only static speckle.

$$\langle I_1 \rangle = I_{\text{obj}} + I_{\text{ref}} + 2\sqrt{I_{\text{obj}}I_{\text{ref}}}\langle\cos(\phi_0 + \xi\sin\omega_0 t)\rangle, \tag{5}$$

where the angled brackets are used to denote an average over the integration time of the detector. Unless the period of the motion of the object is comparable to or greater than the integration time of the detector, the intensity recorded by the detector can be well described as a time average of the two-beam interference over the period of the object's motion. The time-averaged portion of Eq. (5) can be expanded to yield

$$\langle\cos(\phi_0 + \xi\sin\omega_0 t)\rangle = \frac{\cos(\phi_0)}{T}\int_0^T \cos(\xi\sin\omega_0 t)\mathrm{d}t$$
$$-\frac{\sin(\phi_0)}{T}\int_0^T \sin(\xi\sin\omega_0 t)\mathrm{d}t, \tag{6}$$

where T is the integration time of the detector. The second integral in Eq. (6) vanishes, and the integration of the remaining term reduces Eq. (6) to

$$\langle I_1 \rangle = I_{\text{obj}} + I_{\text{ref}} + 2\sqrt{I_{\text{obj}}I_{\text{ref}}}\cos(\phi_0)J_0(\xi), \tag{7}$$

where J_0 is the zero-order Bessel function of the first kind [7].

Although each image recorded by the detector can be expressed in terms of simple two-beam interference, to extract the information both the object and the reference beams must have a constant phase relationship. Unless this is true, phase difference ϕ_0 will vary as a function of position, and the resulting image will not contain the characteristic fringe patterns typically associated with coherent two-beam interference. Thus, to correctly interpret the image, one must know ϕ_0 at each point on the detector.

Since the object under investigation must be diffusely reflecting and illuminated by coherent light, the image will contain a random speckle pattern due to the fact that ϕ_0 varies randomly across the image plane, and any information about the motion of object will be difficult to obtain. To alleviate this problem it is normal to obtain an image before the onset of harmonic motion and subtract it from the subsequent image described by Eq. (7). The intensity at a point on the image plane before the object is set into simple harmonic motion is given by

$$I_2 = I_{\text{ref}} + I_{\text{obj}} + 2\sqrt{I_{\text{ref}}I_{\text{obj}}}\cos\phi_0, \tag{8}$$

and upon subtraction of the two images and subsequent rectification, the intensity of the final interferogram at a point is given by

$$I_{1,2} = 2\sqrt{I_{\text{obj}}I_{\text{ref}}}|\cos(\phi_0)[1 - J_0(\xi)]|. \tag{9}$$

At this point it is useful to consider more than an infinitesimal point on the detector. All detectors sample a finite area of the interfering waves, and the phase difference between the two waves varies as a function of position, resulting in the presence of speckle. Even when the experimental arrangement assures that the average speckle size is equal to the size of the detector (which is usually a single pixel on a CCD array), the size of the speckle is randomly distributed about this mean value so that the response of the detector is normally described by an average over some spatially varying function of phase angle ϕ_o. Additionally it is common to average several measurements of the intensity made at different times to reduce the annoying visual effects attributable to speckle. Since it is reasonable to assume that the value of ϕ_0 will be uniformly distributed, the recorded intensity can be approximated by an average over all possible values. Alternatively, one could record several images and select only the peak intensity from each part of the image for display. In either case the term $\cos\phi_o$ in Eq. (9) can be replaced by a positive constant.

In practice the final values derived from the detector are multiplied by a constant and then displayed on a computer monitor or printed page. Therefore, from a practical standpoint, the multiplicative constants are not important unless they are very close to zero. It is useful to collect all the constants into a single parameter β, which then emphasizes the functional form of the final interferogram, i.e.,

$$I_{1,2} = \beta|1 - J_0(\xi)|. \tag{10}$$

According to Eq. (10), interferograms recorded using the technique described here display points with no displacement ($\xi = 0$) as black, while contours of equal nonzero displacement are denoted by white or gray. Thus the maximum contrast is always unity. However, due to the nature of the Bessel function, the visibility of contiguous contour lines describing an antinodal region decreases as the amplitude of the motion of the surface increases. A plot of Eq. (10) is shown in Fig. 2, which clearly demonstrates that the fringe visibility decreases significantly with increasing displacement of the object.

There are numerous reports of methods to enhance the contrast and usefulness of this type of interferometer. Of particular importance are techniques that shift the phase of one of the beams or the object between images [8–11]. Recording multiple images with known phase shifts between them can not only increase fringe visibility, but it also allows one to determine the relative phases of different parts of a vibrating object unambiguously.

One of the problems with this interferometer is that motion attributable to ambient vibrations can significantly shift the phase of the object beam over the integration time of the detector or between the time of acquisition of the first image and any subsequent image. Such phase shifts decorrelate the object
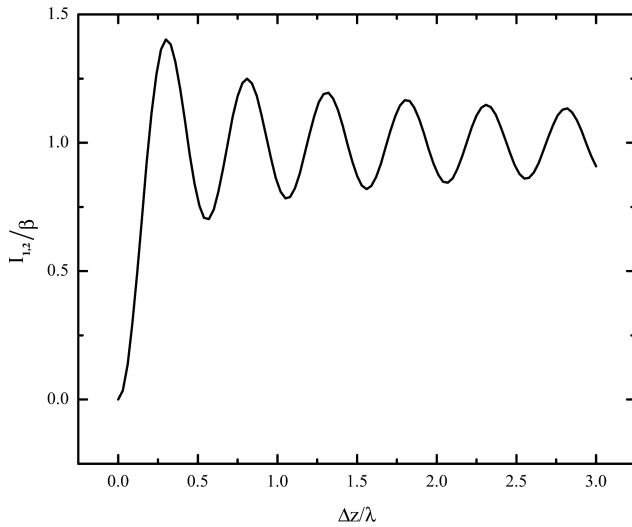
Fig. 2. Plot of the intensity of an electronic speckle pattern interferogram versus the displacement of the object for the interferometer described in Subsection 2.A.

and the reference beams, spoiling the visibility of the final interferograms; therefore, careful isolation from ambient vibrations is an important requirement for this interferometer. de Groot has theoretically investigated the errors that result from ambient vibration and shown that if the noise spectrum is known, it is sometimes possible to perform phase-shifting interferometry without vibration isolation [12]; however, as a general rule, ambient vibrations that result in significant motion of the object will render the electronic speckle pattern interferometer useless. Normally, time-averaged electronic speckle pattern interferometry is not used for objects with significant nonharmonic motion; instead, high-speed cameras or pulsed lasers are used to minimize the adverse effects [13].

B. Electronic Speckle Pattern Interferometer in the Presence of Ambient Motion

The necessity for careful isolation is one of the primary drawbacks of the electronic speckle pattern interferometer. The relative displacement of the interferometer and the object (apart from the intended harmonic motion under investigation) must be significantly less than a wavelength of the illuminating light, or the speckle becomes decorrelated. A lack of sufficient isolation results in the visibility of the fringes approaching zero, and therefore, as time progresses after obtaining the initial image, it is common for the fringes to disappear. The time between the initial image and the final image can often be up to several seconds, depending on the level of isolation, but when the object and interferometer are not mounted on the same support mechanism, the time can be reduced to milliseconds. In this latter case the ability to view fringes becomes highly unlikely, simply because it takes more time to perform the necessary image processing than is available before the object and reference beams become decorrelated.

In what follows we describe a method that allows the electronic speckle pattern interferometer to be used in some situations where ambient vibrations cause the relative motion of the interferometer and object to exceed the subwavelength limit. We assume that the relative motion of the object is due to low-frequency vibrations so that the motion over the integration time of the detector is linear. That is, while the relative motion between the object and the interferometer may be periodic, the period of the motion is much longer than the integration time of the detector. Likewise, should the ambient motion be random, we assume that the mean time between changes in the direction of motion is much longer than the integration time of the detector.

With this assumption, the analysis presented in the previous section is modified by the addition of a linear term in the phase difference between the object and the interferometer so that it is now described by

$$\phi = \phi_0 + \gamma t + \xi \sin \omega_0 t, \tag{11}$$

where

$$\gamma = 2(\vec{v} \cdot \vec{k}), \tag{12}$$

$\vec{v}$ is the velocity of the object due to ambient motion, and $\vec{k}$ is the wave vector of the incident light. Substituting Eq. (11) into Eq. (1), we find that the average intensity recorded at a point on the detector is given by

$$\langle I_n \rangle = I_{\mathrm{obj}} + I_{\mathrm{ref}} + 2\sqrt{I_{\mathrm{obj}} I_{\mathrm{ref}}} \langle \cos(\phi_n + \gamma t + \xi \sin \omega_0 t) \rangle. \tag{13}$$

Since the initial phase angle will change with each measurement, we have introduced subscript n to indicate that we are referring to a specific measurement by the detector. In an experiment this would indicate the specific pixel value in the nth image.

By expanding the cosine term in Eq. (13) and carrying out the time average over the integration time of detector T, the functional form of the interference becomes

$$\langle \cos(\phi_0 + \gamma t + \xi \sin \omega_0 t) \rangle = \frac{\cos(\phi_n)}{T}$$
$$\int_0^T \cos(\gamma t + \xi \sin \omega_0 t) \mathrm{d}t - \frac{\sin(\phi_n)}{T}$$
$$\int_0^T \sin(\gamma t + \xi \sin \omega_0 t) \mathrm{d}t, \tag{14}$$

which is similar to Eq. (6), except that there is a linear term within the arguments of the trigonometric functions. Unfortunately the second integral does not identically vanish as it does without the linear term in the phase. Furthermore when $\gamma T / 2\pi$ is not an integer, Eq. (14) has no known closed-form solution.

Even without solving the integrals in Eq. (14), it is apparent that subtracting an image described by Eq. (13) from an image derived before the onset of harmonic motion will not generally result in interference fringes corresponding to contour lines of equal displacement of the object. The term that is linear in time serves to change the initial phase angle at the onset of integration as well as changing the phase during the integration process. Therefore one would expect that the nonharmonic motion of the object will decorrelate the object and the reference beams, resulting in an interferogram that is difficult, if not impossible, to interpret. However, if one changes the image processing technique, information about the harmonic motion of the object may be retrieved.

To ensure that high-quality interferograms result under these conditions, the two images that are to be subtracted must be recorded while the object is undergoing harmonic motion. That is, rather than subtracting an image of the vibrating object from one recorded before the onset of the motion, both images must be recorded after the onset of harmonic motion. In this case both images have intensities described by Eq. (13).

The ability to observe interference fringes when both images are recorded while the object is harmonically vibrating rests on the assumption that speckle in the nodal portions of the object will have different intensities at different times due to the ambient motion, while the portions of the object that are moving with harmonic motion can still be approximated by Eq. (10). Thus portions of an object where $\Delta z = 0$ will appear bright, while harmonically vibrating portions will appear as contours of dark rings.

To investigate the results of this process, we consider the intensity recorded by a detector at two different times, t and t', both occurring after the onset of harmonic vibration of the object. The two intensities denoted as I_m and I_n are subtracted, and after rectification the resulting intensity is given by

$$
\begin{aligned}
I_{mn} &= |\langle I_m \rangle - \langle I_n \rangle| \\
&= \beta|\langle \cos(\phi_m + \gamma t + \xi \sin \omega_0 t) \rangle \\
&\quad - \langle \cos(\phi_n + \gamma t' + \xi \sin \omega_0 t' \rangle|,
\end{aligned} \tag{15}
$$

where as before β is a constant that depends on the details of the display. Assuming that the two intensities are recorded by the detector contiguously in time, the change in the phase angle can be closely approximated by the phase difference due to the displacement of the object between the two images. Therefore

$$
\phi_n = \phi_m + \gamma T. \tag{16}
$$

Under this assumption Eq. (15) can be rewritten as

$$
\begin{aligned}
I_{mn} = \beta|&\langle \cos[\phi_m + \gamma T\tau + \xi \sin(\omega_0 T\tau)]\rangle \\
&- \langle \cos[\phi_m + \gamma T(1+\tau) + \xi \sin\{\omega_0 T(1+\tau)\}]\rangle|,
\end{aligned} \tag{17}
$$

where $\tau = t/T$ and is bounded by zero and unity.

For the reasons cited in Subsection 2.A, it is necessary to either integrate over all values of initial phase angles ϕ_m or assume the phase angle that produces the maximum intensity, depending on how the image is processed. Assuming that several of the final images will be averaged, Eq. (17) can be explicitly written as

$$
\begin{aligned}
I_{mn} = \beta \int_0^{2\pi} \Big| &\frac{1}{T}\int_0^1 \cos[\phi_m + \gamma T\tau + \xi \sin\{\omega_0 T(\tau)\}]\mathrm{d}\tau \\
&- \frac{1}{T}\int_0^1 \cos[\phi_m + \gamma T(1+\tau) \\
&+ \xi \sin\{\omega_0 T(1+\tau)\}]\mathrm{d}\tau \Big| \mathrm{d}\phi_m.
\end{aligned} \tag{18}
$$

Should one wish to record only the highest value of the intensity, the average over ϕ_m can be replaced by assuming $\phi_m = 0$. Once this is decided the time averages in Eq. (17) can be numerically integrated to determine the resulting intensity at the detector, but the result depends critically on the value of γT. A plot of Eq. (18) versus $\Delta z/\lambda$ for several different values of γT is shown in Fig. 3. The results are insensitive to the frequency of the harmonic vibration as long as ω_o is significantly greater than $2\pi/T$. For the purposes of Fig. 3, the integration time of the detector is assumed to be five times the period of the harmonic vibration of the object so that $\omega_o = 10\pi/T$.

The results shown in Fig. 3 demonstrate that despite the linear motion of the object, interference fringes due to the harmonic motion will still be visible. Furthermore, when compared to Fig. 2, it becomes clear that both the precision and the
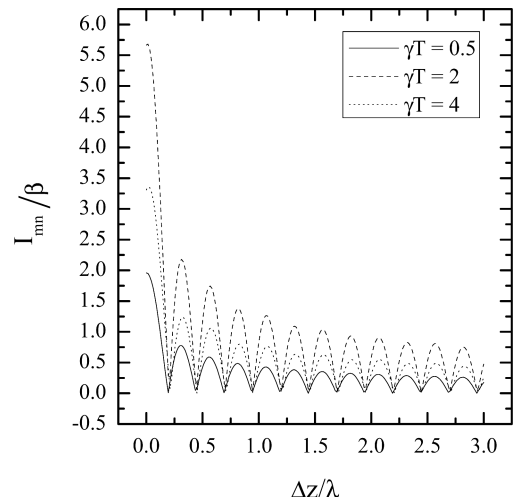
Fig. 3. Plot of the intensity of an electronic speckle pattern interferogram versus the displacement of the object for the interferometer described in Subsection 2.B for three different values of γT.

contrast of this interferometer are superior to one in which there is no relative motion between the object and the interferometer.

In the analysis of the system reported in [4] it was assumed that $\gamma T \ll \xi$ and $\omega_o \gg T^{-1}$; therefore the difference between two contiguous measurements of intensity could be approximated simply by replacing the initial phase ϕ_n in Eq. (15) by $\phi_m + \gamma T$ so that both images can be described by Eq. (4) but with different initial phases. That is, if γ is small enough, the motion of the object can be ignored during the integration time of the detector, but the shift in position of the object between measurements results in a phase shift of γT. The validity of this approximation clearly depends on the value of both γ and T, but for small values of γT, it can be a good approximation. Figure 4 contains plots of Eq. (18) for several values of small γT along with plots of the same equation where it is assumed that $\gamma t = 0$ and $\phi_n = \phi_m + \gamma T$. Note that the approximation is extremely good for $\gamma T < 1$, and depending on the application, it may be acceptable for values exceeding $\gamma T \sim 2$.

The results shown in Fig. 3 also demonstrate that a tolerably wide range of values of γT exists that will produce acceptable interferograms. In fact, an examination of Eq. (18) reveals that the visibility of the fringes is unity for all $\gamma T > 0$. However, this does not mean that the interferometer is useful for that entire range, because the intensity of the interference fringes changes drastically.

The visibility remains high for values of $\gamma T > 0$ due to the fact that the minima of Eq. (18) are consistently zero regardless of the value of γT, although the maximum intensity is cyclic in nature. Figure 5 contains a plot of the maximum value of I_{mn} as a function of γT normalized to the maximum value, which occurs at $\gamma T = 2.32$. As one would expect, when γT is a multiple of 2π, the maximum intensity is reduced to zero; however, with the exception of values that are close to integer multiples of 2π, the interferometer can be used for almost any value of γT. The ability to actually utilize the interferometer for large values of γT depends on the noise floor of the detector. Therefore one may assume that the highest quality interferogram is the one in which the intensity is the greatest when $\Delta z = 0$. This is easily calculable and also provides a relatively simple method for verifying the validity of Eq. (18).

By considering only the special case of viewing nodal regions of the object ($\Delta z = 0$), Eq. (17) reduces to

$$I_{mn}(\Delta z = 0) = \beta|\langle\cos[\phi_m + \gamma T\tau]\rangle$$
$$- \langle\cos[\phi_m + \gamma T(1 + \tau)]\rangle|. \quad (19)$$

Equation (19) indicates that if there is no linear motion of the object, $\gamma = 0$, the pixel intensity of interferograms at nodal regions is identically zero regardless of the value of Δz. However, any nonzero value of γT will result in a nonzero value of Eq. (19).
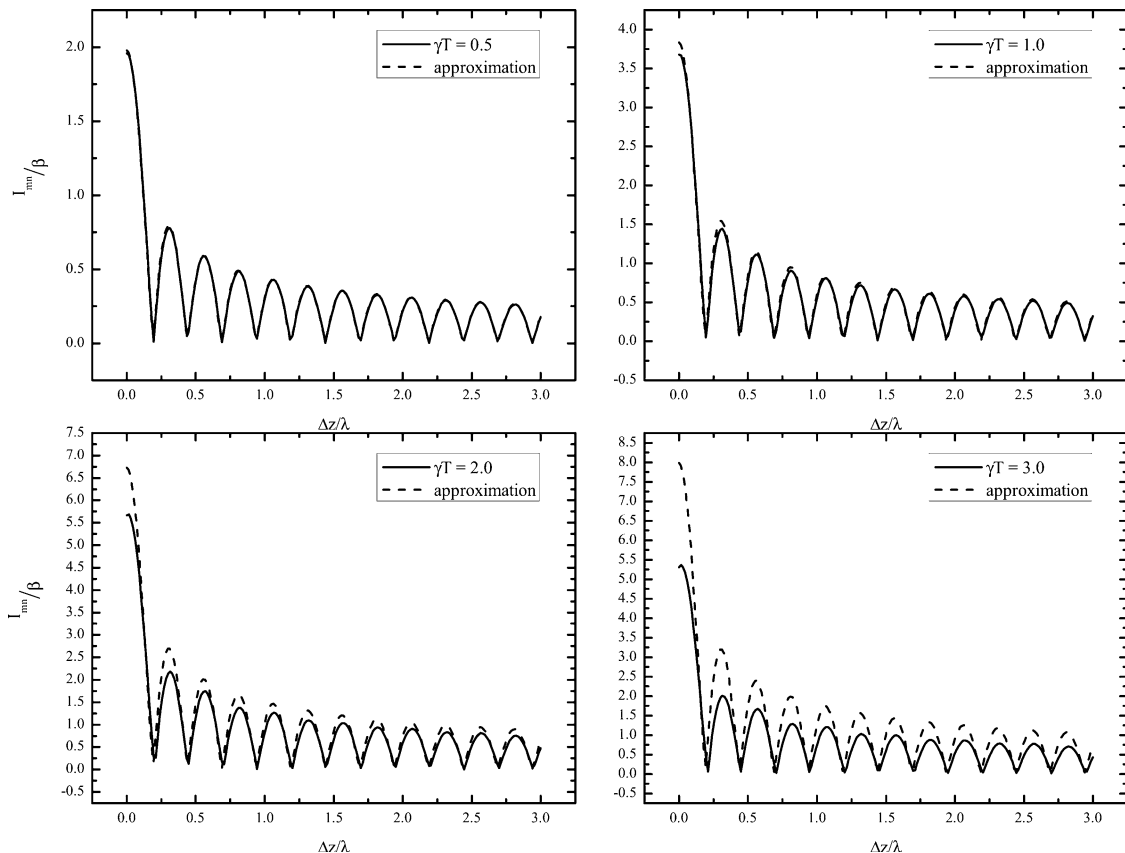

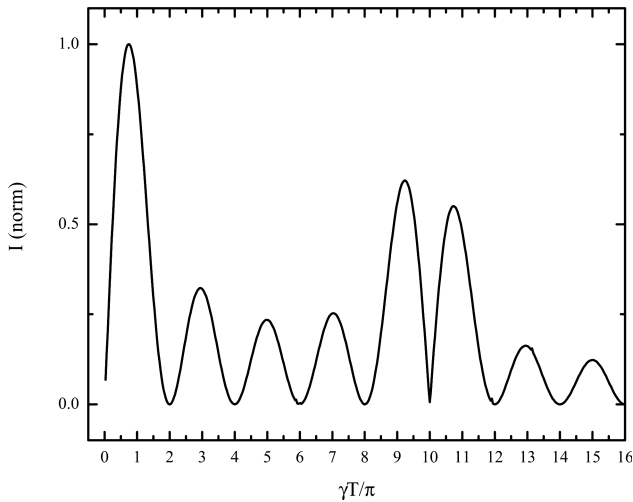Fig. 4. Comparison of the exact and approximate solution to Eq. (18) for four different values of γT.

Fig. 5. Normalized plot of the maximum value of I_{mn} versus γT. Note that there will almost always be some steady-state interference observable as long as γT is not an even-integer multiple of π.

Since the visibility remains high regardless of the value of γT, optimizing the output of the interferometer becomes an issue of maximizing Eq. (19). Carrying out the time averages in Eq. (19) explicitly leads to an equation for the intensity at nodal regions that is only dependent upon γT:

$$I_{mn} = \frac{\beta}{\gamma T} \int_0^{2\pi} |2\sin(\phi_m + \gamma T) - \sin(\phi_m + 2\gamma T) - \sin(\phi_m)| \mathrm{d}\phi_m. \tag{20}$$

Note that, as before, we have integrated Eq. (20) over all possible values of ϕ_m. This describes the intensity of the region of interest when the speckle is not resolved by the detector, or equivalently, when the region of interest is comprised of many detectors (as may be the case when the detector is a two-dimensional array).

Maximizing Eq. (20) in terms of γT provides an indication of the optimum value for actual use. Also, plotting I_{mn} versus γT provides a description of the behavior of the interferometer that can be easily measured. This will be discussed in the following section.

3. Experiments

To verify the validity of the above analysis, we constructed an electronic speckle pattern interferometer shown schematically in Fig. 6 [5,6]. The beam from a He–Ne laser with a wavelength of 632.8 nm was split into two beams by directing it toward a half-wave plate and polarizing beam splitter (PBS). One of the beams was directed through an expanding lens and toward a metal plate sprayed with white paint. The second beam was used as a reference beam, and after the plane of polarization was rotated by a half-wave plate, it was directed toward a beam expanding lens and then onto a piece of opal glass. The reference beam and the object were imaged onto a CCD array simultaneously using a commercially available lens
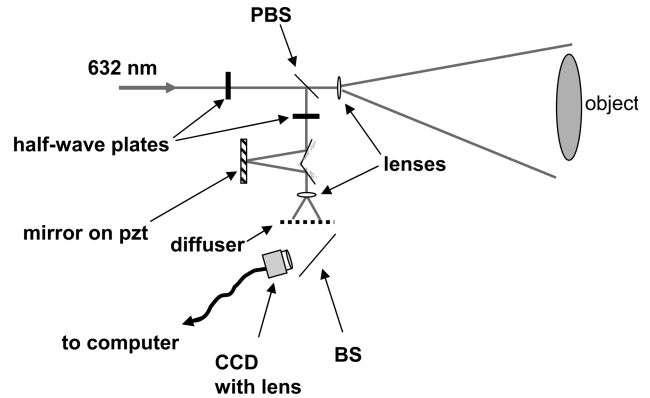

Fig. 6. Diagram of the experimental arrangement.

and a beam splitter. The integration time of the array provided by the manufacturer was $T = 0.0313$ s.

To introduce a known time-varying phase shift onto one of the beams, one of the mirrors used to reflect the reference beam was mounted on a piezoelectric transducer (pzt), which was driven by a triangular waveform. Thus, although the object was not moving relative to the interferometer, the movement could be simulated by a movement of the mirror, and the value of γT could be known precisely. Under these conditions the intensity of the interferogram of the object is given by Eq. (20).

The actuated mirror was driven over a range of velocities, and the average intensity of a region of the recorded interferograms was determined for each velocity. To determine the average intensity of the interferogram, a rectangular region containing 6622 pixels was used. Intensities of pixels within the selected region were averaged, and the average pixel intensity over this region was recorded for each interferogram. For each velocity of the mirror, the average pixel intensity over the selected region was determined for fifteen separate interferograms. Figure 7 contains a plot of these measurements versus γT, along with the theoretical predictions of Eq. (20).
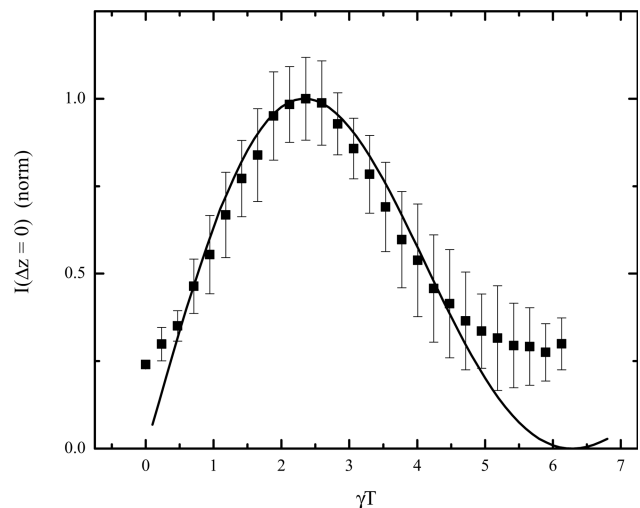

Fig. 7. Comparison of the average intensity of a nodal region of an object ($\Delta z = 0$) to the predictions of Eq. (20).

Note the excellent agreement between the measurements and the theory.

It is also useful to compare the images of this type of interferometer with the more common type described in Subsection 2.A. This provides a vivid example of the ability of the interferometer to work under the conditions described above as well as demonstrating the advantages of inserting a time-varying phase shift in one beam if there is little motion of the object due to effective vibration isolation.

Figure 8 contains two images of a 13 cm diameter flat circular plate vibrating in one of the fundamental modes. The oscillation of the plate was driven acoustically by a speaker placed approximately 1 m away. The amplitude of the vibrations of the antinodes are approximately $0.5\,\mu m$. Figure 8(a) contains an interferogram obtained in the manner described in Subsection 2.A; Fig. 8(b) contains an interferogram obtained in the manner described in Subsection 2.B with the total phase shift of the beam being equivalent to a linear displacement of the plate of approximately $\lambda/4$ over the time of the exposure. The increased precision and visibility are obvious.

4. Discussion

The work discussed above clearly demonstrates that it is possible to perform time-averaged electronic speckle pattern interferometry in the presence of ambient motion, provided that the motion can be assumed to be linear over the integration time of the detector. Experience has proved this to be the usual case for many objects that are not actively isolated from the environment when the integration time of
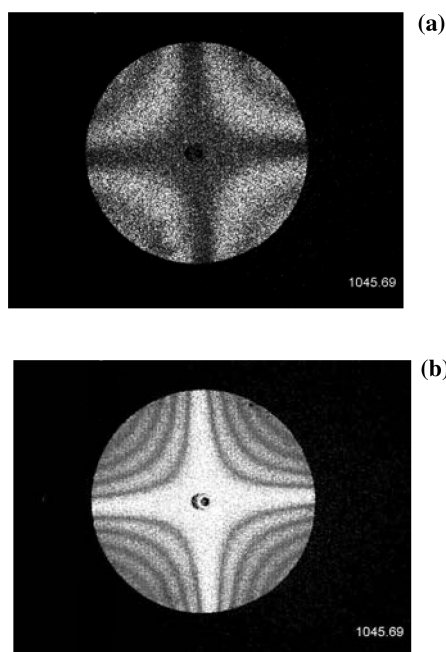
(a)

(b)

Fig. 8. Electronic speckle pattern interferograms of a flat circular plate oscillating in one of the normal modes obtained using the interferometers described in (a) Subsection 2.A and (b) Subsection 2.B. The numbers in the lower right corner of the interferograms indicate the frequency of oscillation ($1045.69 \pm 0.01\,\mathrm{Hz}$).

the detector is of the order of $0.03\,\mathrm{s}$. Furthermore if low-frequency ambient vibrations are not present, it can be advantageous to introduce a time-varying phase shift into one beam of the interferometer to increase the fringe visibility and precision of the interferometer. The data shown in Fig. 7 indicate that the maximum intensity of a nodal region is produced for $\gamma T = 2.4 \pm 0.1$, which is in good agreement with the value of $\gamma T = 2.32$ predicted by Eq. (20). These results also demonstrate the importance of the noise floor of the detector. The noise floor of the detector used for the experiments described above is normal for an inexpensive, uncooled CCD array. However, despite the obvious noise inherent in the detector, the images shown in Fig. 8 demonstrate that excellent interferograms can be produced.

Numerical integrations of Eq. (18) have also shown that it is not necessary to completely restrict the ambient motion such that it is linear over the integration time of the detector. Depending on the magnitude of the motion, interference fringes may be visible for ambient harmonic motion up to a large fraction of ω_o, although the relationship between the fringes and the displacement of the object may become complicated. Likewise, if the ambient motion is complex or random, but so rapid that Eq. (11) is not a good approximation, averaging several interferograms will still produce an image with fringes corresponding to contours of equal displacement.

Finally, due to the manner in which most detectors operate, the theory presented in Subsection 2.B assumes that the initial phase angle between the two subtracted images is γT [Eq. (16)]; however, this need not necessarily be the case. In some cases decoupling the initial phase angle from the period of integration of the detector can offer possibilities to maximize the contrast of the final image. By not assuming the phase angle is defined by Eq. (16), but instead that the initial phase angle ϕ_n can be controlled through a judicious choice of time delay between images, the initial phase of the nth image can be described by

$$\phi_n = \phi_m + \gamma T', \tag{21}$$

where T' need not be related to the integration time of the detector. In some circumstances this may offer an additional opportunity to maximize the intensity of nodal regions of the interferogram, but if the final result is the average of many images, the time delay between images becomes unimportant, and the results do not depend critically on the value of T'.

5. Conclusion

In the past the use of electronic speckle pattern interferometry has typically been restricted to laboratory settings due to the stringent requirements for vibration isolation. The experimental arrangement described here relaxes this requirement and makes it possible to use speckle pattern interferometry in a variety of situations where vibration isolation is

complicated or expensive. This work does not indicate that the need for vibration isolation can always be eliminated; high-frequency ambient vibrations should still be minimized to produce the maximum fringe visibility. However, because much of the difficulty in using electronic speckle pattern interferometry to study large, weakly supported, or independently supported objects can be traced to low-frequency motion, the method described here can often be used to produce interferograms in situations heretofore deemed too difficult to attempt.

We note in closing that there is no reason to limit the application of this interferometer to cases where degradation of the image is due to terrestrial motion as has been the emphasis here. This interferometer may have application in instances where the presence of any source of optical path variation makes interferometry of a harmonically vibrating object difficult. Provided the path variation meets the criteria specified above, the interferometer can be used in the presence of environmental disturbances such as air flow or thermal drift and can eliminate the deleterious effects attributable to such things as the inadvertent motion of optical components.

References

1. R. Jones and C. Wykes, *Holographic and Speckle Interferometry*, 2nd Ed. (Cambridge, 1989).
2. P. K. Rastogi, *Speckle Pattern Interferometry and Related Techniques* (Wiley, 2001).
3. D. Findeis, D. R. Rowland, and J. Gryzagoridis, "Vibration isolation techniques suitable for portable electronic speckle pattern interferometry," Proc. SPIE **4704**, 159–167 (2002).
4. T. R. Moore and S. A. Zietlow, "Interferometric studies of a piano soundboard," J. Acoust. Soc. Am. **119**, 1783–1793 (2006).
5. T. R. Moore, "A simple design for an electronic speckle pattern interferometer," Am. J. Phys. **72**, 1380–1384 (2004).
6. T. R. Moore, "Erratum: a simple design for an electronic speckle pattern interferometer," Am. J. Phys. **73**, 189 (2005).
7. M. Abramowitz and I. A. Stegun, eds., *Handbook of Mathematical Functions* (Dover, 1972).
8. S. Nakadate, "Vibration measurement using phase-shifting speckle-pattern interferometry," Appl. Opt. **25**, 4162–4167 (1986).
9. K. A. Stetson and W. R. Brohinsky, "Fringe-shifting technique for numerical analysis of time-averaged holograms of vibrating objects," J. Opt. Soc. Am. A **5**, 1472–1476 (1988).
10. C. Joenathan, "Vibration fringes by phase stepping on an electronic speckle pattern interferometer: an analysis," Appl. Opt. **30**, 4658–4665 (1991).
11. C. Joenathan and B. M. Khorana, "Contrast of the vibration fringes in time-averaged electronic speckle-pattern interferometry: effect of speckle averaging," Appl. Opt. **31**, 1863–1870 (1992).
12. P. J. de Groot, "Vibration in phase-shifting interferometry," J. Opt. Soc. Am. A **12**, 354–365 (1995).
13. A. J. Moore, J. D. C. Jones, and J. D. R. Valera, "Dynamic measurements," in *Speckle Pattern Interferometry and Related Techniques*, P. K. Rastogi, ed. (Wiley, 2001), pp. 225–288.